

The G11.11-0.12 Infrared-Dark Cloud: Anomalous Dust and a Non-Magnetic Isothermal Model

Doug Johnstone¹, Jason D. Fiege¹, R.O. Redman¹, P.A. Feldman¹, and Sean J. Carey²

ABSTRACT

The G11.11-0.12 Infrared-Dark Cloud has a filamentary appearance, both in absorption against the diffuse $8\mu\text{m}$ Galactic background, and in emission from cold dust at $850\mu\text{m}$. Detailed comparison of the dust properties at these two wavelengths reveals that standard models for the diffuse interstellar dust in the Galaxy are not consistent with the observations. The ratio of absorption coefficients within the cloud is $\kappa_8/\kappa_{850} \leq 1010$, which is well below that expected for the diffuse ISM where $\kappa_8/\kappa_{850} \sim 1700$. This may be due to the formation of ice mantles on the dust and grain coagulation, both of which are expected within dense regions of molecular clouds. The $850\mu\text{m}$ emission probes the underlying radial structure of the filament. The profile is well represented by a marginally resolved central region and a steeply falling envelope, with $\Sigma(r) \propto r^{-\alpha}$, where $\alpha \geq 3$, indicating that G11.11-0.12 is the first observed filament with a profile similar to that of a non-magnetic isothermal cylinder.

Subject headings: ISM:clouds - ISM:dust,extinction - ISM:evolution - ISM:structure - ISM:individual objects:G11.11-0.12

1. Introduction and Observations

Infrared-dark clouds (IRDCs) have been identified by their substantial mid-infrared ($8\text{--}25\mu\text{m}$) extinction in *Midcourse Space Experiment* (MSX) images (Egan et al. 1998). Egan et al. concluded from the high mid-infrared opacities of the IRDCs that they possess hundreds of magnitudes of visual extinction and contain large column densities of cold dust. They

¹National Research Council Canada, Herzberg Institute of Astrophysics, 5071 West Saanich Rd, Victoria, BC, V9E 2E7, Canada; doug.johnstone@nrc-crnc.gc.ca, jason.fiege@nrc-crnc.gc.ca, russell.redman@nrc-crnc.gc.ca, paul.feldman@nrc-crnc.gc.ca

²SIRTf Science Center, California Institute of Technology, Mail Code 220-6, Pasadena, CA 91125; carey@ipac.caltech.edu

derived characteristic physical parameters for the gas inside the IRDCs: $l \approx 0.5 - 15$ pc, $T_K \approx 10 - 20$ K, $n(\text{H}_2) \geq 10^5 \text{ cm}^{-3}$, and H_2 column densities ranging up to 10^{23} cm^{-2} (Carey et al. 1998).

A number of IRDCs have been mapped with SCUBA on the JCMT (Carey et al. 2000; Redman et al. 2000, 2003) and are found to have the mid-infrared absorption closely associated with filamentary and/or flocculent clouds in emission at 850 and $450 \mu\text{m}$. Bright, compact sources with masses in the range ≈ 10 to $10^3 M_\odot$ and infall/outflow signatures are located along the filaments and appear to be in a variety of the early stages of star formation. The larger IRDCs appear to be similar in size to the Orion molecular cloud but different in many important aspects. They are more heavily extinguished, colder, more quiescent, and at earlier stages of evolution.

For the work reported in this paper, we investigate the IRDC G11.11-0.12, at a kinematic distance of 3.6 kpc (Carey et al. 1998), because it contains several long, filamentary segments seen against a relatively uniform galactic background at $8 \mu\text{m}$ (Fig. 1). Carey et al. (2000) first reported JCMT observations of this source. Star formation appears to be more active in the southern part of the cloud than the northern half, with bright, compact SCUBA sources (labelled P1, P6 and P7 in Fig. 2). The P1 source is driving a molecular outflow and is associated with a weak point source of $8 \mu\text{m}$ emission. There is no evidence of high-mass star formation throughout most of the cloud. The catalog of Becker et al. (1994) lists two UCHII regions in the vicinity of G11.11-0.12, but they are far enough away that they are unlikely to be affecting the IRDC properties even if they are at the same distance.

JCMT³ SCUBA observations were obtained at $850 \mu\text{m}$ under fair weather conditions ($\tau_{850} = 0.24 - 0.30$) in April 1999 with an angular resolution of $14.5''$. “Scan mapping” was employed to produce Nyquist-sampled images. The data were taken with the standard observing set-up using chop throws of $20''$, $30''$ and $65''$ at position angles of 0° and 90° . The data were processed using the JCMT data reduction pipeline (ORAC) to flatfield, extinction correct and calibrate the chop data (Economou et al. 1999; Jenness & Economou 1999). The calibration accuracy is good to $\pm 15\%$ (Jenness et al. 2002). The optimal map reconstruction (see Fig. 2) was then performed from the individual chop measurements, using a matrix inversion technique outlined by Johnstone et al. (2000). Slowly varying spatial features with wavelengths much longer than the maximum chop, $65''$, are not measured reliably; thus, large, low-amplitude structures in the reconstructed map tend to be artifacts. Further

³The JCMT is operated by the Joint Astronomy Centre on behalf of the Particle Physics and Astronomy Research Council of the UK, the Netherlands Organization for Scientific Research, and the National Research Council of Canada

descriptions of SCUBA and its observing modes can be found in Holland et al. (1999) and Jenness et al. (2000).

Heterodyne observations of ^{13}CO (2–1) and C^{18}O (2–1) were taken near the P2 region of G11.11-0.12 with receiver RxA3 on the JCMT during several observing sessions in July 2000, April 2001, and June 2001. The velocity dispersion within the cloud can be estimated by fitting single component Gaussians to the line profiles. Typical linewidths obtained have $\sigma = 1.2 \text{ km s}^{-1}$ for the ^{13}CO line and $\sigma = 0.9 \text{ km s}^{-1}$ for the C^{18}O line. The temperature of the gas in the segment of the filament labelled P2 (Fig. 2) has been estimated from H_2CO observations by Carey et al. (1998) to be less than 20 K.

2. Dust Properties: Extinction versus Emission

The extinction of background emission at $8\mu\text{m}$ is due to the presence of dust within the G11.11-0.12 filament. This same dust radiates at submillimeter wavelengths and is observable as emission in the $850\mu\text{m}$ image. It is expected that there should be a strong correlation between the extinction and emission maps, and this is indeed seen in Figs. 1 and 2. The correlation is complicated by several factors: (1) the diffuse background emission at $8\mu\text{m}$, which the molecular cloud extinguishes, is not entirely smooth; (2) star formation occurring at P1 produces $8\mu\text{m}$ emission; (3) the zero submillimeter emission baseline is poorly defined; (4) the measured emission and absorption properties are beam-convolved; (5) the dust temperature and emissivity may change with location in the cloud because the degree of dust coagulation and freeze-out of molecules onto grain mantles depend on the local physical conditions, such as density and temperature.

Statistically relevant results can be obtained by analyzing a large sample of measurements, despite the above caveats. Fig. 3 shows the $8\mu\text{m}$ emission versus the $850\mu\text{m}$ emission for each location across the filament, along with the median $8\mu\text{m}$ flux as a function of $850\mu\text{m}$ emission. The trend in both the data and the median curve is clear: the $8\mu\text{m}$ flux decreases due to extinction as the $850\mu\text{m}$ flux increases. The highest $850\mu\text{m}$ emission points do not follow this trend because of the presence of an energetic protostellar source (P1) within the deepest part of the cloud that is altering the temperature of the dust and producing weak $8\mu\text{m}$ emission.

Given the clear trends in Fig. 3, a simple dust model may be fit to the data. At each location \mathbf{x} across the filament, the measured $8\mu\text{m}$ flux density $f_8(\mathbf{x})$ depends on an unvarying foreground $f_8(\text{fg})$ and background $f_8(\text{bg})$ emission, and the optical depth through the cloud $\tau_8(\mathbf{x}) = \kappa_8 \Sigma(\mathbf{x})$, where κ_λ is the absorption coefficient of the gas plus dust at wavelength

$\lambda(\mu\text{m})$ and $\Sigma(\mathbf{x})$ is the column density of material within the intervening cloud. Explicitly,

$$f_8(\mathbf{x}) = f_8(\text{bg}) \exp[-\kappa_8 \Sigma(\mathbf{x})] + f_8(\text{fg}). \quad (1)$$

The column density of the cloud is related to the the observed flux density $f_{850}(\mathbf{x})$ (measured in Jy/beam), for the optically thin submillimeter emission, by the equation

$$f_{850}(\mathbf{x}) = B_{850}(T_d) \kappa_{850} \Sigma(\mathbf{x}) \Omega, \quad (2)$$

where $B_\lambda(T_d)$ is the Planck function at λ and Ω is the solid angle subtended by the telescope beam. Thus, the optical depth at $8\mu\text{m}$, which is given by $\tau_8(\mathbf{x}) = k f_{850}(\mathbf{x})$, is linearly related to the observed flux at $850\mu\text{m}$, with k defined by $\kappa_8/\kappa_{850} = k B_{850}(T_d) \Omega$.

The correlation between the flux at $8\mu\text{m}$ and $850\mu\text{m}$ in Fig. 3 allows for a determination of k (and $f_8(\text{bg})$, $f_8(\text{fg})$). The overlaid dashed line in Fig. 3 is based on the best-fit model, with $k = 3.75$, $f_8(\text{bg}) = 2.3 \times 10^{-6} \text{ W m}^{-2} \text{ sr}^{-1}$, and $f_8(\text{fg}) = 2.5 \times 10^{-6} \text{ W m}^{-2} \text{ sr}^{-1}$. Excellent fits are found for a small range around $k = 3.75 \pm 0.25$, implying

$$\frac{\kappa_8}{\kappa_{850}} \simeq \frac{1350}{\exp(17 \text{ K}/T_d) - 1}. \quad (3)$$

Observations of molecular lines provide a range of gas temperatures, $T_K \approx 10 - 20 \text{ K}$, with a best-fit value of $T_K = 15 \text{ K}$. Theoretical models of the dust temperature toward highly extinguished cloud centers (Zucconi et al. 2001; Evans et al. 2001; Kramer et al. 2003) yield lower limits of $5 - 8 \text{ K}$. The corresponding limits on the opacity ratio are 1010 if $T_d = 20 \text{ K}$ and 50 if $T_d = 5 \text{ K}$.

For diffuse interstellar dust the expected opacity ratio is ~ 1700 (Li & Draine 2001); however, ice mantles form on the surfaces of dust grains in dense molecular clouds and the grains themselves coagulate. This increases the submillimeter opacity and obscures the silicate features that account for most of the opacity at $8\mu\text{m}$ (Ossenkopf & Henning 1994). Ossenkopf and Henning found that, after 10^5 yrs of coagulation, dust with thin ice mantles entrained in cold ($T_K < 20 \text{ K}$) gas with number density $n = 10^6 \text{ cm}^{-3}$ produced an opacity ratio between $8\mu\text{m}$ and $850\mu\text{m}$ of ~ 500 , consistent with these observations if the dust temperature is $T_d \simeq 13 \text{ K}$. Kramer et al. (2003) found a similar increase in the importance of submillimeter emission compared to (near) infrared extinction in the filamentary cloud IC 5148. These result are consistent with evidence for dust growth in cold, dense protoplanetary disks where observations of the slope of the spectral energy distribution are used (Li & Lunine 2003)

All reasonable dust models require a foreground $8\mu\text{m}$ emission of $f_8(\text{fg}) \sim f_8(\text{bg})$ which implies that half of the diffuse mid-infrared emission is produced *in front* of the filament.

This is intriguing given that G11.11-0.12 is only 3.6 kpc away and on the near side of the Galactic Center. The diffuse $8\mu\text{m}$ emission, while relatively uniform across the IRDC, must be significantly patchy on Galactic scales.

3. The Filamentary Structure of G11.11-0.12

The simplest equilibrium model for a filament is that of an isothermal cylinder (Ostriker 1964) where the density profile as a function of cylindrical radius r is given by

$$\rho = \frac{\rho_c}{(1 + r^2/8r_0^2)^2}, \quad (4)$$

where ρ_c is the central density and r_0 is the core radius defined by $\sigma^2 = 4\pi G \rho_c r_0^2$. The velocity dispersion σ should be derived from the temperature of the gas for a true isothermal cylinder. However, in most astrophysical cases the measured velocity dispersion within the molecular cloud includes a significant “non-thermal” (turbulent) component.

The surface density profile for an edge on isothermal cylinder is:

$$\Sigma = \frac{\Sigma_0}{(1 + r^2/8r_0^2)^{3/2}}, \quad (5)$$

where $\Sigma_0 = 2^{1/2} \pi \rho_c r_0$. The surface density profile becomes $\Sigma \propto r^{-3}$, at large projected distances from the center of the cylinder.

Most studied filamentary clouds are not well-fit by this profile. L97 in Cygnus (Alves et al. 1998), the Integral Shaped Filament (ISF) in Orion A (Johnstone & Bally 1999), IC5146 (Lada et al. 1999), and a quiescent filament in Taurus (Stepnik et al. 2003) are all better fit by shallow density profiles with $\rho \propto r^{-2}$, which are consistent with surface density profiles of $\Sigma \propto r^{-1}$. Such profiles are well-fit by the Fiege & Pudritz (2000) model, which features a helical magnetic field. The r^{-2} density profile is obtained in FP models with a dominant toroidal field component, but steeper profiles are possible when the poloidal field dominates. Submillimeter polarization measurements trace the geometry of the magnetic field and provide additional evidence in support of the FP helical field model, which has been shown to agree with polarization maps of the ISF (Matthews et al. 2001) and NGC2024 (Matthews et al. 2002).

The radial structure of two well-defined regions of the G11.11-0.12 filament, a northern segment including P3 and P4, and a southern segment including P1 and P2, have been analyzed. The average intensity distributions orthogonal to the spine of the filament were determined using the same technique as applied to the ISF (Johnstone & Bally 1999), and

are presented in Fig. 4. The G11.11-0.12 segments appear similar to each other, with a marginally resolved central region connecting to an outer region characterized by a density profile steeper than r^{-3} . This is in contrast to results for the ISF where the central region is unresolved, and whose surface density only falls off as $r^{-1.0 \pm 0.25}$ at large radii $r \gg r_0$ (Johnstone & Bally 1999).

The emission from each section of G11.11-0.12 is reasonably fit by an isothermal profile (dashed lines in Fig. 4) allowing for an estimation of the core radius r_0 . The core radius varies from $r_0 = 0.12 \pm 0.02$ pc in the northern segment to $r_0 = 0.10 \pm 0.02$ pc in the southern segment (assuming a 3.6 kpc distance to G11.11-0.12). The measured peak flux is $f_0 = 0.20 \pm 0.03$ Jy/beam and $f_0 = 0.43 \pm 0.06$ Jy/beam, respectively, where the uncertainty in the peak flux is primarily due to uncertainties in the $850\mu\text{m}$ calibration. The observed dust emission can be converted to a central surface density Σ_0 , despite uncertainty in both the dust temperature and emissivity, using

$$\Sigma_0 = 0.13 \left(\frac{f_0}{1 \text{ Jy/beam}} \right) \left(\frac{\kappa_{850}}{0.02 \text{ cm}^2 \text{ g}^{-1}} \right)^{-1} [\exp(17 \text{ K}/T_d) - 1] \text{ g cm}^{-2}. \quad (6)$$

Assuming a typical dust temperature of 13 K, a gas-to-dust ratio of 100, and a dust emissivity $\kappa_{850} = 0.02 \text{ cm}^2 \text{ g}^{-1}$ (Ossenkopf & Henning 1994), the central surface density is $0.07 \pm 0.01 \text{ g cm}^{-2}$ in the northern segment and $0.15 \pm 0.02 \text{ g cm}^{-2}$ in the southern segment. If the dust temperature were much lower, the column density would be significantly larger.

The central number density of H_2 atoms can also be derived from the profile:

$$n_c = 2.6 \times 10^4 \left(\frac{f_0}{1 \text{ Jy/beam}} \right) \left(\frac{r_0}{0.1 \text{ pc}} \right)^{-1} \left(\frac{\kappa_{850}}{0.02 \text{ cm}^2 \text{ g}^{-1}} \right)^{-1} [\exp(17 \text{ K}/T_d) - 1] \text{ cm}^{-3}. \quad (7)$$

For the canonical dust properties, $n_c = 1.1 \pm 0.3 \times 10^4 \text{ cm}^{-3}$ in the northern segment, and $n_c = 3.3 \pm 0.7 \times 10^4 \text{ cm}^{-3}$ in the southern segment. The measured C^{18}O linewidth observed for G11.11-0.12 near the location of P2 is $\sigma = 0.9 \text{ km/s}$, allowing for an independent measure of the central density, $n_c = 3.4 \pm 0.6 \times 10^4 \text{ cm}^{-3}$, via the core radius definition. The agreement between these two derivations of central density provides support for the isothermal model. However, more complex filamentary models, including poloidal and toroidal magnetic components, may produce as good or better fits to the data (Fiege et al. 2003).

4. Discussion and Conclusions

G11.11-0.12 is the first molecular filament observed to have a radial density profile steeper than r^{-3} at large radii $r \gg r_0$. A non-magnetic isothermal cylinder model (Ostriker

1964) provides a reasonable fit to both the profile and the measured constraints: submillimeter flux, temperature, velocity dispersion, and core radius. The data might also be consistent with the generalized magnetic Stodolkiewicz model (Stodólkiewicz 1963; Nakamura et al. 1993), whose density profile is identical to that of the Ostriker model, except that the core radius definition takes into account the effects of a helical magnetic field. The data are not consistent with the toroidally dominated regime of the FP model, which results in much more shallow density profiles (Fiege & Pudritz 2000). Work is in progress to provide a detailed parameter space exploration and numerical fits to the Ostriker model, the generalized Stodolkiewicz model and the full range of the FP model, including the steep profiled regime that is dominated by the poloidal field component.

The IRDCs are thought to be a cold, dense, and quiescent class of molecular clouds (Egan et al. 1998; Carey et al. 1998, 2000). The dust properties measured for G11.11-0.12 between the mid-infrared and the submillimeter are consistent with this interpretation; however, the theoretical models of Ossenkopf & Henning (1994) require approximately 10^5 yrs for grain coagulation to become important and thus place a lower limit on the lifetime of the cloud. The dynamical time of a self-gravitating non-magnetic isothermal filament, $t_d \simeq (G\rho_c)^{-1/2}$, on which the filament might be expected to fragment and form stars, is similar to the crossing time $t_c \simeq 2r_0/\sigma$, which can be calculated directly from the observations; $t_c \simeq 2 \times 10^5$ yrs. Thus, the required coagulation time does not pose severe constraints on the equilibrium of the filament. It is harder to reconcile the filament’s moderate central density $n_c = 1 - 4 \times 10^4 \text{ cm}^{-3}$, which is well below the value of 10^6 cm^{-3} assumed by Ossenkopf and Henning in their coagulation calculations. It is possible that the dense gas in the core of the filament is clumped. Further studies of the correlation between $8\mu\text{m}$ extinction and submillimeter emission in this and other IRDCs should prove beneficial.

REFERENCES

- Alves, J., Lada, C.J., Lada, E.A., Kenyon, S.J., & Phelps, R. 1998, *ApJ*, 506, 292
- Becker, R.H., White, R.L., Helfand, D.J., & Zoonematkermani, S. 1994, *ApJS*, 91, 347
- Carey, S.J., Clark, F.O., Egan, M.P., Price, S.D., Shipman, R.F., & Kuchar, T.A. 1998, *ApJ*, 508, 721
- Carey, S.J., Feldman, P.A., Redman, R.O., Egan, M.P., MacLeod, J.M., & Price, S.D. 2000, *ApJ*, 543, L157
- Economou, F., Bridger, A., Wright, J.S., Jenness, T., Currie, M.J., Adamson, A. 1999, in

- Astronomical Data Analysis Software and Systems VIII, ASP Conf. Ser. Vol. 172, eds. D.M. Mehringer, R.L. Plante, D.A. Roberts, (San Francisco: ASP), p.11
- Egan, M.P., Shipman, R.F., Price, S.D., Carey, S.J., Clark, F.O., & Cohen, M. 1998, ApJ, 494, L199
- Evans, N.II, Rawlings, J., Shirley, Y., & Mundy, L. 2001, ApJ, 557, 193
- Fiege, J.D. & Pudritz, R.E. 2000, ApJ, 544, 830
- Fiege, J.D., Johnstone, D., Redman, R.O., Feldman, P.A., & Carey, S. 2003, ApJ, in preparation
- Holland, W.S., et al. 1999, MNRAS, 303, 659
- Jenness, T. & Economou, F. 1999, in Astronomical Data Analysis Software and Systems VIII, ASP Conf. Ser. Vol. 172, eds. D.M. Mehringer, R.L. Plante, D.A. Roberts, (San Francisco: ASP) , p.171
- Jenness, T., Lightfoot, J.F., Holland, W.S., Greaves, J.S., & Economou, F. (2000), in Imaging at Radio through Submillimeter Wavelengths, eds. J. Mangum & S. Radford (San Francisco: ASP), p.205
- Jenness, T., Stevens, J.A., Archibald, E.N., Economou, F., Jessop, N.E., & Robson, E.I. 2002, MNRAS, 336, 14
- Johnstone, D. & Bally, J. 1999, ApJ, 510, L49
- Johnstone, D., Wilson, C.D., Moriarty-Schieven, G., Creighton, J.G., & Gregersen, E. 2000, ApJS, 131, 505
- Kramer, C., Richter, J., Mookerjee, B., Alves, J., & Lada, C. 2003, A&A, 399, 1073
- Lada, C.J., Alves, J., & Lada, E.A. 1999, ApJ, 512, 250
- Li, A. & Draine, B.T. 2001, ApJ, 554, 778
- Martin, P.G. & Whittet, D.C.B. 1990, ApJ, 357, 113
- Li, A. & Lunine, J.I. 2003, ApJ, in press
- Matthews, B.C., Fiege, J.D., & Moriarty-Schieven, G. 2002, ApJ, 569, 304
- Matthews, B.C. & Wilson, C.D. 2000, ApJ, 531, 868

- Matthews, B.C., Wilson, C.D. & Fiege J.D. 2001, ApJ, 562, 400
- Nakamura, F., Hanawa, T., & Nakano, T. 1993, PASJ, 45, 551
- Ossenkopf, V. & Henning, Th. 1994, A&A, 291, 943
- Ostriker, J. 1964, ApJ, 140, 1056
- Redman, R.O., Feldman, P.A., Carey, S.J., & Egan, M.P. 2000, in Star Formation from the Small to the Large Scale, Proc. 33rd ESLAB Symp. ESA SP-445, eds. F. Favata, A.A. Kaas, & A. Wilson, p.499
- Redman, R.O., Feldman, P.A., Wyrowski, F., Côté, S., Carey, S.J., & Egan, M.P. 2003, ApJ, 586, 1127
- Stepnik, B. et al. 2003, A&A, 398, 551
- Stodólkiewicz, J.S. 1963, Acta Astron., 13, 30
- Zucconi, A., Walmsley, C.M., & Galli, D. 2001, A&A, 376, 650

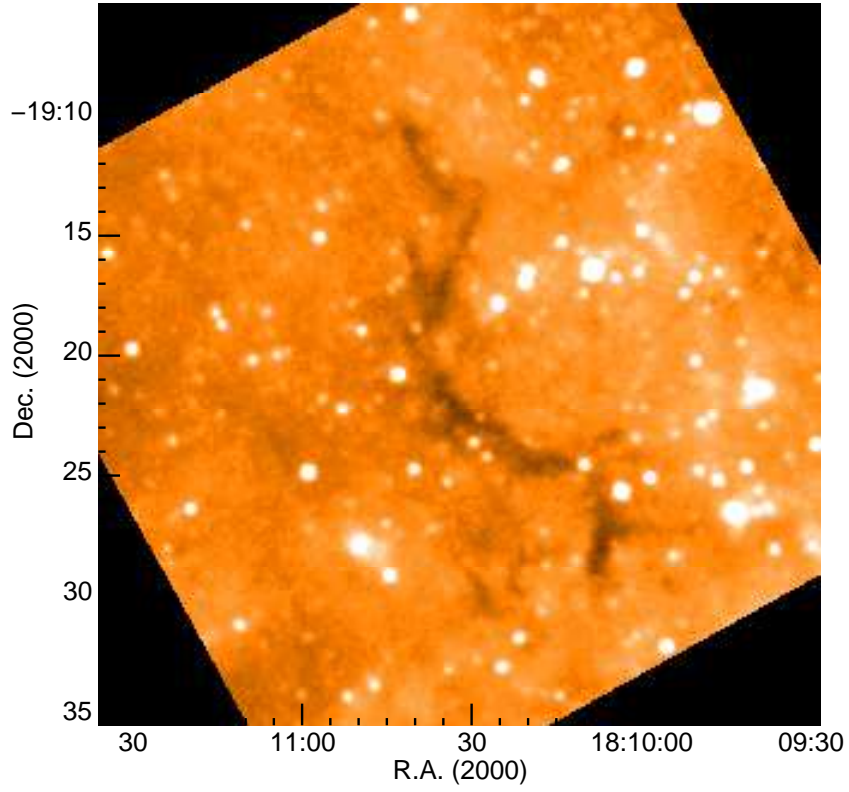


Fig. 1.— MSX $8\mu\text{m}$ image showing the mid-infrared emission in the direction of G11.11. Note the narrow filamentary extinction lane.

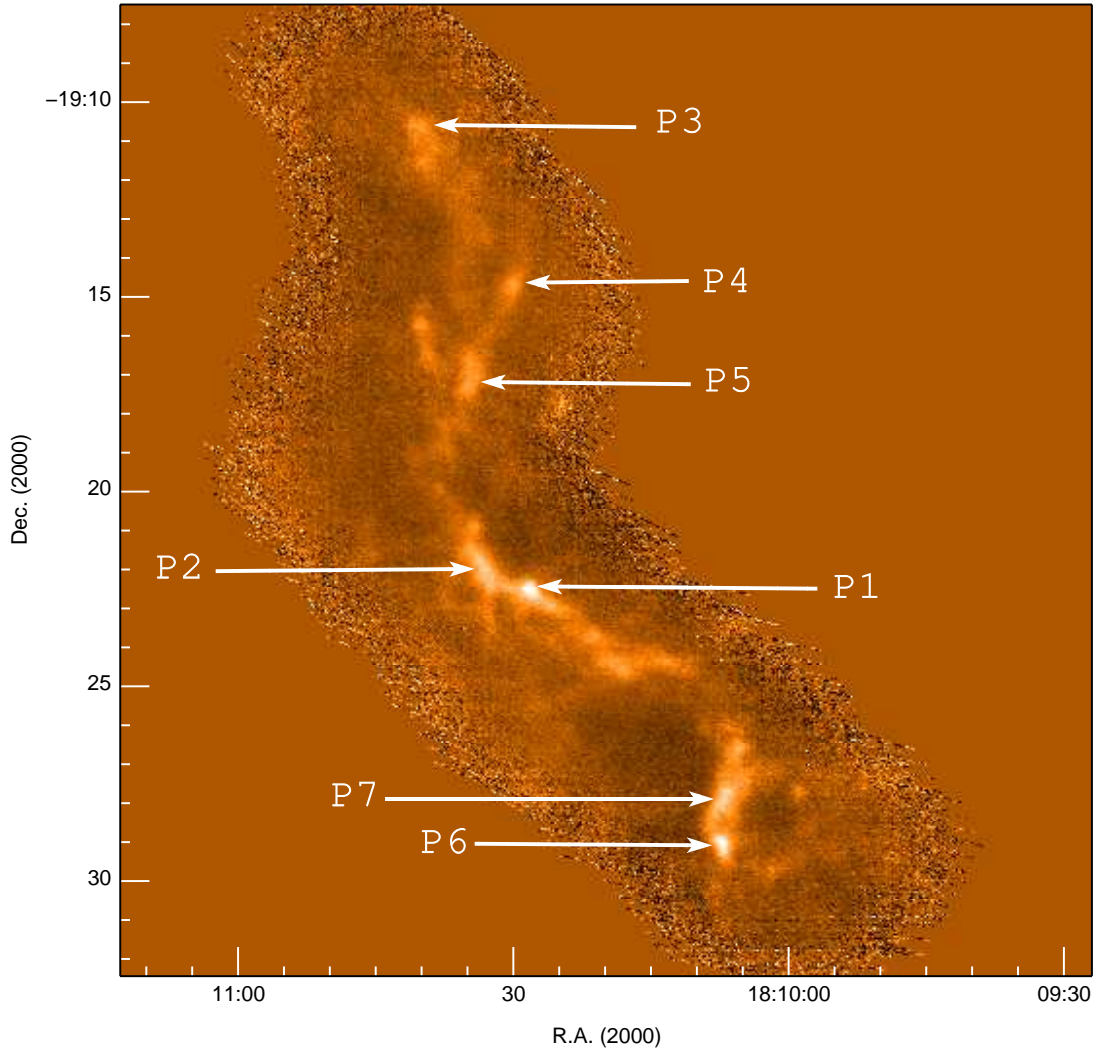


Fig. 2.— 850 μm emission in the direction of G11.11. The intensity range is from -0.1 to 0.7 Jy/beam. Note the strong correlation between the submillimeter dust emission and the mid-infrared extinction in Fig. 1.

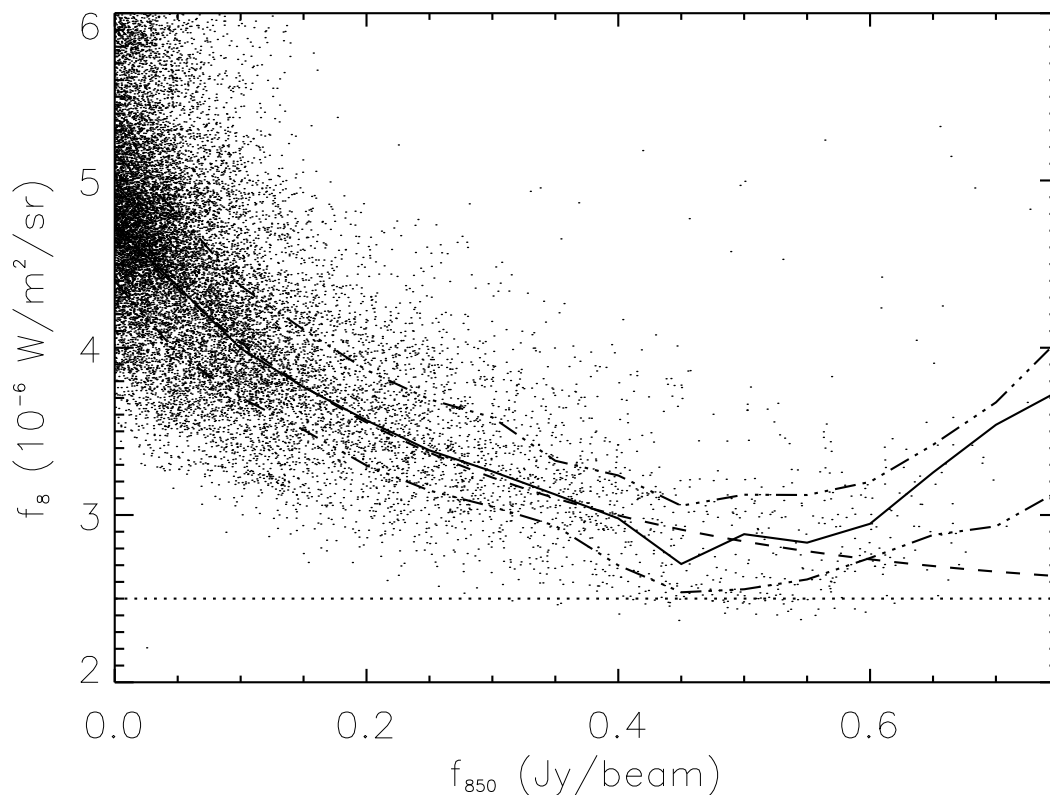


Fig. 3.— Measured $8\mu\text{m}$ flux versus $850\mu\text{m}$ flux at each position within the G11.11 filament. The solid line indicates the median $8\mu\text{m}$ flux as a function of $850\mu\text{m}$ flux while the dashed-dotted lines give the range containing 50 percent of the $8\mu\text{m}$ measurements. The overlaid dashed line represents the best-fit model (see text) with the dotted line marking the required $8\mu\text{m}$ foreground flux $f_s(\text{fg}) = 2.5 \times 10^{-6} \text{ W m}^{-2} \text{ sr}^{-1}$. Note that the fit becomes poor at large $850\mu\text{m}$ flux due to the presence of a warm source at P1, producing internal $8\mu\text{m}$ emission.

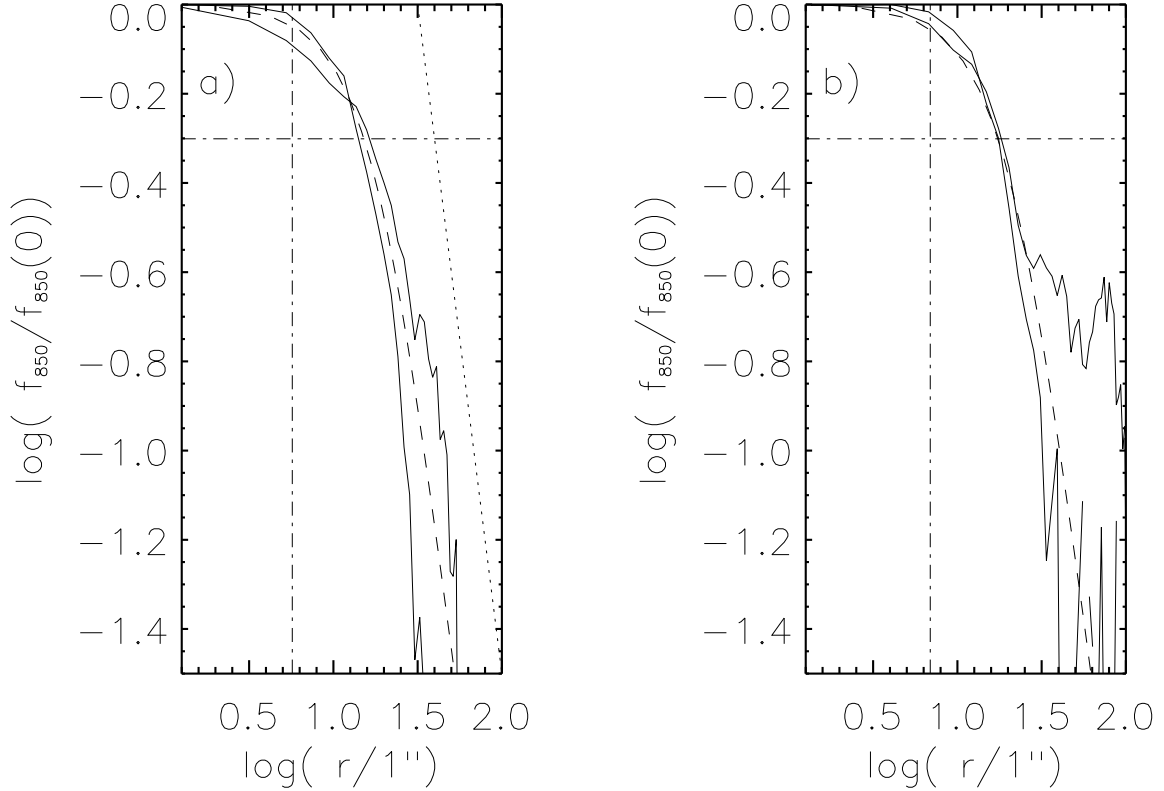


Fig. 4.— $850\mu\text{m}$ emission profile across the G11.11 filament measured at two locations: (a) southern segment, (b) northern segment. In each panel, the two solid lines show independently the left and right profile from the ridge center. The overlaid curved dashed line represents the column density profile of an isothermal cylinder with $r_0 = 0.10\text{ pc}$ (southern segment) and $r_0 = 0.12\text{ pc}$ (northern segment) after convolution by the $14.5''$ beam of the JCMT. The dash-dotted lines denote where the flux is half the peak value and the radius corresponding to the $14.5''$ beam. The dotted line in panel (a) shows a power-law relation with $f \propto r^{-3}$, equivalent to the asymptotic isothermal profile. In panel (b), the flattening of one profile is due to the proximity of a second filamentary spur.